chemosensors

MDPI

Article

Theoretical Study of 3d VIII Atom-Decorated γ-Graphyne for Adsorbing and Detecting Heptafluoroisobutyronitrile

Ziang Zheng [1,†], Renchu Zhao [1,†], Dachang Chen [1,*], Qing Miao [1], Ke Liu [1] and Beibei Xiao [2]

[1] School of Electrical and Electronic Engineering, Wuhan Polytechnic University, Wuhan 430023, China; zza7850162@163.com (Z.Z.); zhaorenchu2022@163.com (R.Z.); miaoq@whpu.edu.cn (Q.M.); liuke@whpu.edu.cn (K.L.)

[2] School of Energy and Power Engineering, Jiangsu University of Science and Technology, Zhenjiang 212003, China; xiaobb11@mails.jlu.edu.cn

* Correspondence: dcchen@whpu.edu.cn

† These authors contributed equally to this work.

Abstract: Recently, Heptafluoroisobutyronitrile (C_4F_7N) has received widespread attention in replacing one of the most greenhouse-insulating gas, SF_6. However, gas leakage is incredibly harmful to the health of operational personnel and the security of industry production, and developing C_4F_7N detection technology is of great necessity. In this work, the adsorption properties, as well as the sensing performance of C_4F_7N on 3d VIII atom-decorated γ-graphyne (γ-GY), were theoretically discussed. The adsorption structures, adsorption energies, electron transfer, adsorption distance, electron distribution, and electronic properties were compared. The results show that the introduction of Fe and Co atom enhance the chemisorption of C_4F_7N, and the adsorption of C_4F_7N brings the maximum electron redistribution of Fe/γ-GY among three TM/γ-GY. Only the adsorption on Fe/γ-GY leads to the vanishing of the magnetic moment and creates a band gap. For three different modifications of γ-GY, the chemical interactions are highly related to the overlapping of transition metal 3d and N 2p orbitals in the density of states. The adsorption on Co/γ-GY causes the maximum change in work function from 5.06 eV to 5.26 eV. In addition, based on the band structure, work function, and desorption properties, the sensing properties of 3d VIII atom-decorated γ-GY were evaluated in order to promote the experimental exploration and development of high-performance C_4F_7N gas sensors.

Keywords: density functional theory; C_4F_7N; 3d VIII atom; γ-graphyne; gas sensor

check for updates

Citation: Zheng, Z.; Zhao, R.; Chen, D.; Miao, Q.; Liu, K.; Xiao, B. Theoretical Study of 3d VIII Atom-Decorated γ-Graphyne for Adsorbing and Detecting Heptafluoroisobutyronitrile. *Chemosensors* **2023**, *11*, 411. https://doi.org/10.3390/chemosensors11070411

Academic Editor: Eleonora Alfinito

Received: 22 June 2023
Revised: 17 July 2023
Accepted: 19 July 2023
Published: 21 July 2023

1. Introduction

As one of the most widely used insulating gases in the fields of high voltage and microelectronic etching, SF_6 has excellent dielectric strength and arc-extinguishing characteristics [1,2]. However, SF_6 is one of the most harmful greenhouse gases. Its greenhouse warm potential (GWP) value is about 23,500 times that of CO_2, and the atmospheric life of SF_6 reaches 3200 years [3]. In order to address these drawbacks, a novel insulation gas with environmentally friendly characteristics should be considered and explored. Heptafluoroisobutyronitrile (C_4F_7N), one of the most promising SF_6 alternatives, has been widely investigated as a kind of gas-insulating medium. The GWP of C_4F_7N is only about 2100 with an ozone depletion potential value of 0, and the dielectric strength of C_4F_7N is twice that of SF_6 [4–6]. However, due to its high liquefaction temperature (−4.7 °C), C_4F_7N must be mixed with buffer gas such as CO_2 or N_2 [7]. If the content of C_4F_7N reaches about 18% to 20%, the dielectric strength of the mixed gas can be as high as that of pure SF_6 [6]. Based on the compatibility of insulation performance and environmental friendliness of C_4F_7N mixed gases, they have been widely exploited in medium-voltage and high-voltage gas-insulated equipment [8]. However, C_4F_7N has potential biological toxicity. During the production, operation, and regular maintenance of the insulation equipment, it needs to be

filled or replaced with C_4F_7N mixed gas. In the meantime, production and maintenance staff inevitably come into contact with C_4F_7N. Cytotoxicity tests show that the lethal concentration 50 value (LC50) of C_4F_7N is 1.5%, and the occupational exposure limits derived from the 28-day subacute inhalation toxicity study is only 0.0065% [9]. Based on the LC50 value, C_4F_7N can be classified as Category 4 of the Globally Harmonized System (GHS) of Classification and Labelling of Chemicals [10].

Recently, two-dimensional (2D) materials have a large specific area and numerous active sites, which benefit gas adsorption and sensing [11]. Among 2D carbon allotropies, graphene was first synthesized in 2004 and has attracted a large amount of research attention in various fields, including gas sensors [12–14]. However, due to its zero-band gap property, adjusting the band structure of graphene is relatively difficult [15]. In recent years, a notable carbon allotropy called graphyne (GY) has been predicted and synthesized. GY exhibits remarkable mechanical, optical, and chemical properties due to its hexagonal carbon rings with sp2 hybridization and triple bonds with sp hybridization [16]. Two kinds of GY have been successfully synthesized, including γ-GY and graphdiyne (GDY) [16]. GDY has shown great promise in energy, catalysis, environmental science, electron devices, etc. Previous studies have indicated that γ-GY has the maximum binding energy among the members of the graphyne family and is the most stable structure [17]. However, γ-GY has received less attention due to the difficulty in experimental synthesis. Cui et al. used a cross-coupling reaction through mechanochemistry to synthesize γ-GY with p-type semiconductor properties [18]. Zhang et al. reported a novel reversible dynamic alkyne metathesis method to obtain stacked bulk γ-GY [19]. These experimental reports have inspired subsequent studies to discuss the physical and chemical properties of γ-GY in numerous fields. Due to the limited research on the experimental investigation of γ-GY, most of the studies have focused on theoretical research. The doping of transition metal (TM) atoms or clusters has been proven to be a feasible strategy for controlling the physical properties and surface activity [20–22].

In the realm of gas adsorption and surface reactions, pristine γ-GY shows small adsorption energies for most hazardous molecules (<0.20 eV), such as NH_3, NO, and CO. Therefore, surface modification needs to be considered [23]. To enhance the interactions between γ-GY and small molecules, the introduction of adatoms or substitutional atoms can create active adsorption sites for sensing or catalysis. For example, dispersed TM atoms on γ-GY (also called TM sites) provide adsorption sites and enhance the adsorption strength of CO, thereby facilitating further oxidizing reactions [24]. Moreover, different TM sites lead to different adsorption and catalytic behaviors. Fu et al. compared the adsorption of CO_2 on different TM atoms embedded γ-GY. The adsorption strength is influenced by the type of element and the charge regulation of the system. Additionally, non-noble TMs are more suitable for CO_2 capture and storage applications, which sheds light on the design of TM/γ-GY for gas adsorption [25]. Gan conducted a systematic investigation of different TM atom embedded γ-GY for oxygen reduction and evolution reactions and identified the most promising candidate for bifunctional catalyst [26]. The aforementioned researches provide novel and practical insights for designing high-performance TM/γ-GY for detecting C_4F_7N leaking gas.

Dispersed VIII atoms exhibit excellent adsorption and catalytic performance [26,27]. Furthermore, they have considerable binding energy with substrate materials. Among them, 3d VIII atoms have lower costs and are easy to industrialize. Therefore, in this study, we conducted a theoretical investigation of different 3d VIII atom-decorated γ-GY as sensing materials to adsorb and detect C_4F_7N based on density functional theory (DFT). The optimal adsorption structures of C_4F_7N on Fe, Co, and Ni embedded γ-GY were obtained, and the adsorption behavior was explored by comparing the adsorption energies, electron transfer, adsorption distance, and magnetic properties. Additionally, the electron distribution, band structure, and density of states (DOS) were discussed. To further explore the sensing properties, the work function and desorption behavior were calculated. We believe that our study provides guidance for the design and develop C_4F_7N semiconductor

gas sensors applied in the electric power industry to guarantee the bio-safety of technicist and operations.

2. Methods

All the spin-polarized DFT calculations were performed using the DMol^3 code [28]. The generalized gradient approximation (GGA) method of the Perdew–Burke–Ernzerhof (PBE) approach was chosen to describe the exchange-correlation function [29,30]. In order to account for the weak interactions of C_4F_7N adsorption arising from the Van der Waals force, the long-range interactions were corrected with DFT-D2 proposed by Grimme [31]. The cutoff radii were set to 5.0 Å with the application of double numerical polarization (DNP) basis set realized by DFT semi-core pseudopotential (DSSP). The Monkhorst–Pack k point was set to 3 × 3 × 1 for geometric optimization, while a more accurate grid of 5 × 5 × 1 was used for electronic properties [32]. The convergence criteria between the two steps of geometric optimization were set as follows: an energy difference of 10^{-6} Ha (1 Ha = 27.21 eV), a maximum force of 0.001 Ha/Å, and a maximum displacement of 0.005 Å. The structure of γ-GY was constructed using a 2 × 2 single unit cell, and in order to evaluate the binding strength between a single 3d VIII TM atom and γ-GY, the binding energy was as follows:

$$E_B = E_{TM/\gamma\text{-}GY} - E_{\gamma\text{-}GY} - E_{TM\ atom} \quad (1)$$

where $E_{TM/\gamma\text{-}GY}$, $E_{\gamma\text{-}GY}$, and $E_{TM\ atom}$ are the calculated total energy of a single 3d VIII TM atom embedded γ-GY, pristine γ-GY, and single 3d VIII TM atom.

To calculate the adsorption of C_4F_7N on Fe, Co, and Ni embedded γ-GY, the adsorption energy was defined as follows:

$$E_{ad} = E_{C_4F_7N\ on\ TM/\gamma\text{-}GY} - E_{TM/\gamma\text{-}GY} - E_{C_4F_7N} \quad (2)$$

where $E_{C4F7N\ on\ TM/\gamma\text{-}GY}$ and E_{C4F7N} are the total energy of C_4F_7N molecule adsorbed on TM/γ-GY, C_4F_7N molecule before adsorption. To evaluate the electron transfer of TM adsorbed on pristine γ-GY and C_4F_7N on TM/γ-GY, the charge of every atom of all the systems was obtained based on Hirshfeld analysis [33]. Moreover, to make a deeper investigation of electron transfer between C_4F_7N and TM/γ-GY, the charge density difference (CDD) was calculated as follows:

$$\Delta\rho = \rho_{C_4F_7N\ on\ TM/\gamma\text{-}GY} - \rho_{TM/\gamma\text{-}GY} - \rho_{C_4F_7N} \quad (3)$$

where $\rho_{C4F7N\ on\ TM/\gamma\text{-}GY}$, $\rho_{TM/\gamma\text{-}GY}$, and ρ_{C4F7N} are the total electron density of the C_4F_7N molecule adsorbed on TM/γ-GY, TM/γ-GY, and C_4F_7N molecules before adsorption.

3. Results

3.1. Structure of C_4F_7N, Pristine and 3d VIII Atom-Decorated γ-GY

The structures of C_4F_7N, pristine, and modified γ-GY are shown in Figure 1. The color recognition of different atoms is displayed in Figure 1a, and the optimized structure of C_4F_7N is shown in Figure 1b. Based on the result of the Fukui function, the C≡N bond is identified as the most chemically active bond in C_4F_7N, with the active site located near the top of the N atom, where C_4F_7N exhibits the highest chemical activity [34]. The calculated bond length of C≡N is 1.17 Å, which is consistent with previous research [34,35]. Due to the higher reactivity of the C≡N bond compared to other bonds or groups, only one orientation of C_4F_7N adsorption is considered, with C≡N perpendicular to the adsorption site. For pristine γ-GY, the lattice parameter of 2 × 2 super cell of γ-GY is optimized to be 13.78 Å (6.89 Å for a single unit cell [36,37]), as shown in Figure 1c. To construct the single 3d VIII TM atom decorated γ-GY, one TM atom is placed in the hollow site of the three C≡C acetylenic bonds in one ring. This site has been proven to have the maximum binding energy for Fe, Co, and Ni adatom [20]. The calculated absolute binding energies of Fe, Co, and Ni adatom with pristine γ-GY are 4.57 eV, 5.14 eV, and 5.23 eV, respectively, as

shown in Table 1. These values are higher than the cohesive energies of the bulk phase of these three TM elements (4.28 eV, 4.39 eV, and 4.44 eV), indicating that the single TM atoms (Fe, Co, or Ni) are not likely to form aggregations [20]. The distance between the TM atom and the closest C atom in the ring is 1.97 Å, 1.94 Å, and 1.95 Å, respectively. Regarding the charge analysis, the Fe adatom exhibits the highest positive charge, and Fe and Co display magnetic moments of 2.13 and 1.03 on γ-GY, respectively. This magnetism can be attributed to the orbital mixing between the d orbitals of the TM atoms and the conduction band of γ-GY [38]. After the decoration of a single TM atom, the TM site demonstrates significant adsorption and reaction activity, qualifying it as an active site on γ-GY [26]. Consequently, this study focused specifically on the adsorption of C_4F_7N on the TM site to investigate the sensing performance.

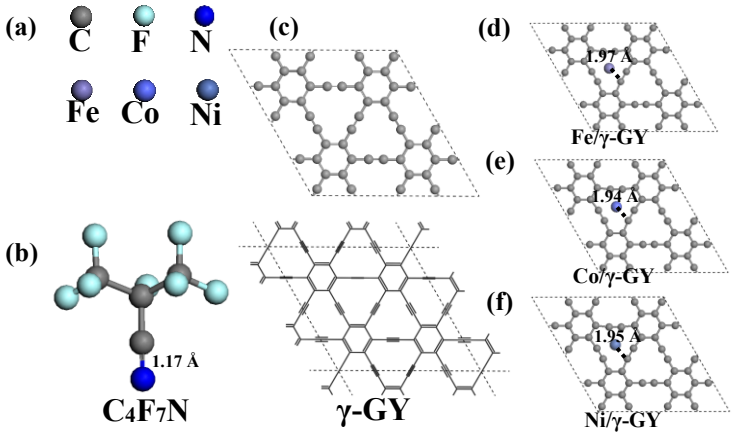

Figure 1. Geometric structures of C_4F_7N, pristine γ-GY, and 3d VIII atom-decorated γ-GY: (**a**) atom specification; (**b**) C_4F_7N; (**c**) pristine γ-GY; (**d**) Fe/γ-GY; (**e**) Co/γ-GY; (**f**) Ni/γ-GY.

Table 1. Binding energy, distance, Hirshfeld charge, and magnetic moment of different TM adatom on γ-GY.

Element	Binding Energy (eV)	Distance (Å)	Hirshfeld Charge (e)	Magnetic Moment of TM Atom (μ_B)
Fe/γ-GY	−4.57	1.97	+0.16	+2.13
Co/γ-GY	−5.14	1.94	+0.07	+1.03
Ni/γ-GY	−5.23	1.95	+0.03	0.00

3.2. Adsorption of C_4F_7N on Different Single 3d VIII TM Atom-Decorated γ-GY

The optimized adsorption structures of C_4F_7N on a single 3d VIII TM atom embedded γ-GY are displayed in Figure 2, and the corresponding adsorption parameters are listed in Table 2. The electronic properties may be affected by the introduction of the U value if using the DFT+U method, but the effect on the adsorption energy is relatively small [39]. Considering the limitations of the current DMol module, the U value is not included in this study, and it does not change the tendency of properties of different TM atoms on γ-GY. When comparing the adsorption parameters of C_4F_7N on different TM atom sites, the absolute adsorption energy of C_4F_7N on the Fe site is significantly higher than that on the Co and Ni site, reaching 1.02 eV, while the adsorption on the Ni site is the lowest, with only 0.28 eV. The adsorption on the Ni site is also compared to the adsorption on pristine γ-GY. The adsorption energy of C_4F_7N on the Ni site is very similar to the adsorption on pristine γ-GY, indicating that the Ni site has a limited effect on promoting the interactions between C_4F_7N and γ-GY. The effects of DFT-D2 dispersion corrections are also evaluated and are listed in Table 2. For Fe/γ-GY, chemical interactions have the most significant effect, while for Ni/γ-GY, most of the interactions are attributed to the Van der Waals force. Based on this observation, the adsorption on the Fe site exhibits evident chemical

interactions, whereas the adsorption on the Co site involves a combination of chemisorption and physisorption. On the other hand, physisorption predominantly contributes to the adsorption on the Ni site. According to Hirshfeld analysis, the values for weak interactions of adsorption are approximately +0.04 e for Ni/γ-GY and pristine γ-GY. For Co/γ-GY, this value is slightly higher (+0.06 e), while it is even smaller for Fe/γ-GY. This phenomenon indicates that the electron transfer value is small for all three adsorptions. The reasons are discussed below.

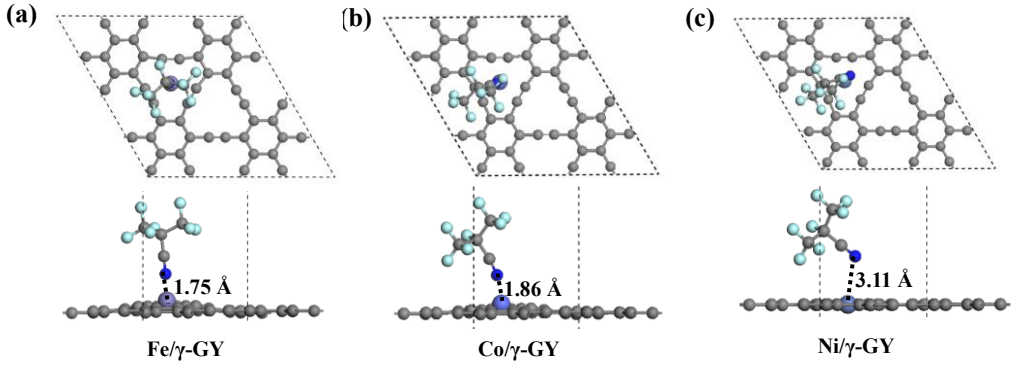

Figure 2. Adsorption structures of C_4F_7N on 3d VIII atom-decorated γ-GY: (**a**) Fe/γ-GY; (**b**) Co/γ-GY; (**c**) Ni/γ-GY.

Table 2. Adsorption energy, electron transfer, and adsorption distance of C_4F_7N on pristine and 3d VIII Atom-decorated γ-GY.

Adsorption Structure	E_{ads} (eV)	E_{ads} with Out DFT-D2 (eV)	Q_T (e)	Magnetic Moment of TM Atom after Adsorption (μ_B)
Fe/γ-GY	−1.02	−0.77	+0.01	0
Co/γ-GY	−0.66	−0.35	+0.06	+0.75
Ni/γ-GY	−0.28	−0.01	+0.04	0
Pristine γ-GY	−0.27	−0.01	+0.04	/

CDD is a useful method for analyzing the charge distribution before and after gas adsorption [40]. To further investigate the electron transfer, CDD configurations are calculated and presented in Figure 3. Since chemisorption on the Fe and Co site is more pronounced, the isosurface value is set to 0.01 e/Å^3, while for Ni/γ-GY, this value is only 0.002 e/Å^3. In the case of Fe/γ-GY, the region between the Fe and N atoms exhibits an encapsulated structure with electron depletion at the center and accumulation surrounding it. The maximum absolute electron density along the Z-axis can reach 40 e/Å^3. Therefore, even though the electron transfer value is small, there is a significant redistribution of the electron cloud for Fe/γ-GY after C_4F_7N adsorption. It is important to note that the Hirshfeld analysis is based on electron density [33], and while chemisorption can result in an obvious redistribution of the electron cloud, it may not necessarily lead to a numerical electric charge. In the case of adsorption on Co/γ-GY, by comparing the maximum value of electron density change, the absolute peak value is only about 15 e/Å^3, indicating a weaker degree of redistribution compared to Fe/γ-GY. Regarding Ni/γ-GY, the redistribution is much less noticeable due to the flat curve shown in Figure 3b. Therefore, stronger adsorption strength leads to more pronounced electron redistribution, but the redistribution is not directly related to the value of electron transfer.

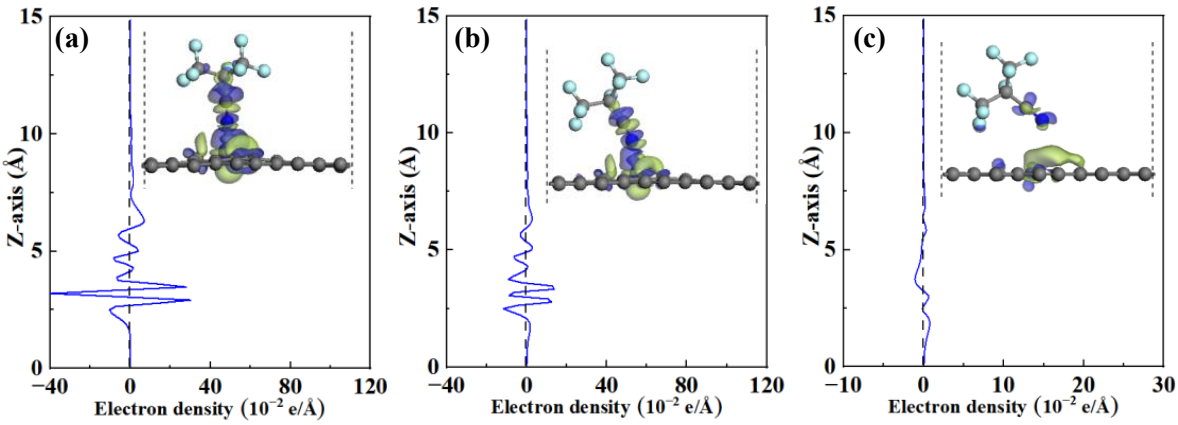

Figure 3. CDD of C_4F_7N on 3d VIII atom-decorated γ-GY: (**a**) Fe/γ-GY (the isosurface of 3D configurations is 0.01 e/Å^3); (**b**) Co/γ-GY (the isosurface of 3D configurations is 0.01 e/Å^3); (**c**) Ni/γ-GY (the isosurface of 3D configurations is 0.002 e/Å^3); the blue region is electron accumulation while yellow region is electron depletion.

3.3. Electronic Properties of Single 3d VIII TM Atom-Decorated γ-GY before and after Adsorbing C_4F_7N

To evaluate the sensing properties, a comparison of the electronic properties of TM atom decorated γ-GY before and after C_4F_7N adsorption was conducted, including the band structure, DOS, and work function. The band structures before and after C_4F_7N adsorption are depicted in Figure 4. Due to the non-zero magnetic moment of Fe/γ-GY and Co/γ-GY, the band structure is split into spin-up and spin-down parts (represented by blue and red curves). Prior to adsorption, Fe/γ-GY and Co/γ-GY both exhibit a zero-band gap, whereas Ni/γ-GY has a small band gap of approximately 0.31 eV, indicating its semiconductor properties. After C_4F_7N adsorption, strong adsorption strength and significant electron redistribution lead to the vanishing of the magnetic moment of Fe/γ-GY and the emergence of a 0.31 eV band gap. The adsorption of C_4F_7N induces substantial changes in the electron configuration of Fe's 3d orbitals, eliminating the presence of unpaired electrons. For Co/γ-GY, the adsorption results in changes in some bands near +1 eV and the Fermi-level. Additionally, the magnetic moment of the Co atom undergoes a minor decrease from +1.03 μ_B to +0.75 μ_B while the structure still exhibits no band gap. Thus, the adsorption of C_4F_7N also modifies the electron configuration of Co's 3d orbitals, although Co still remains a magnetic moment with unpaired electrons. In the case of Ni/γ-GY, the band structure and band gap undergo minimal change, indicating weak effects on the electron configurations of Ni/γ-GY after C_4F_7N adsorption.

To further explore the chemical interactions between adsorbed C_4F_7N and TM atom decorated γ-GY, the total DOS (TDOS), partial DOS (PDOS) of the adsorbed molecules, and DOS of atomic orbitals were calculated and are shown in Figure 5. Before adsorption, due to the non-zero magnetic moment of Fe/γ-GY and Co/γ-GY, their DOS exhibits asymmetrical structures. The PDOSs of the 3d orbitals are depicted in a green shade. The Fe 3d and Co 3d orbitals have some unoccupied states located above 0 eV. In contrast, all Ni 3d orbitals are occupied. After C_4F_7N adsorption, the states of the adsorbed C_4F_7N are shown in Figure 5d–f with orange curves. Since only Co/γ-GY retains a magnetic moment after adsorption, the states of the adsorbed C_4F_7N exhibit an asymmetric structure. Furthermore, for C_4F_7N adsorption on the Fe and Co site, some states appear near 0 eV, indicating orbital interactions between C_4F_7N and TM decorated γ-GY. To further investigate these interactions, the atomic orbitals are presented in Figure 5g–i. For Fe/γ-GY, there are overlapping states between the Fe 3d and N 2p orbitals near −8 eV, ranging from −7 eV to −4 eV, and above 0 eV, at around +1.5 eV, +2 eV, and +3 eV. Similarly, overlapping between the Co 3d and N 2p orbitals is observed near −8 eV, within the range of −7 eV to −4.5 eV, near 0 eV, and from +2 eV to +3 eV. However, Ni/γ-GY exhibits minimal overlapping peaks.

Although there may be some overlapping states from −6 eV to −4 eV, the peak points do not coincide at the same energy value. Additionally, after adsorption, the magnetic moment of Fe/γ-GY vanishes, resulting in the PDOS of the Fe 3d adopting a symmetrical structure. The Co 3d orbitals experience changes near 0 eV after C_4F_7N adsorption. However, because the adsorption on the Ni site is weak, the DOS of the Ni 3d orbitals hardly changes. This phenomenon indicates much weaker chemical interactions between C_4F_7N and the Ni atom. Therefore, when comparing the adsorption of C_4F_7N on different TM decorated γ-GY, Fe and Co atoms contribute to stronger chemical interactions to some extent, while the Ni atom does not enhance the adsorption ability of C_4F_7N on γ-GY.

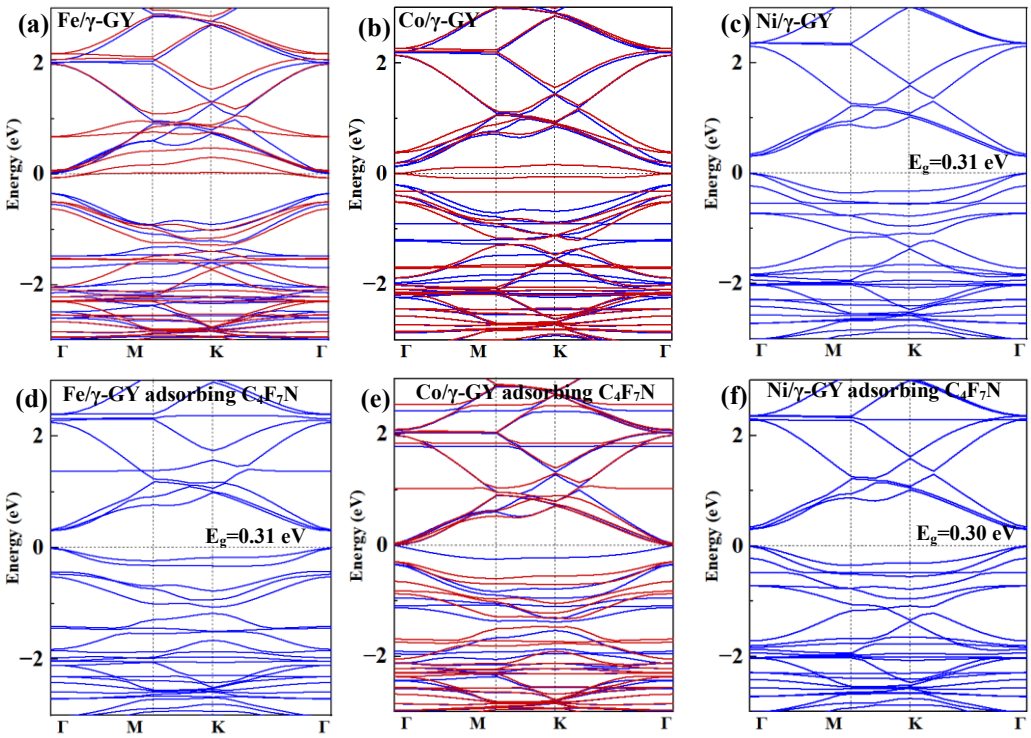

Figure 4. Band structures of 3d VIII atom-decorated γ-GY before and after adsorbing C_4F_7N: (**a**) Fe/γ-GY before adsorption; (**b**) Co/γ-GY before adsorption; (**c**) Ni/γ-GY before adsorption; (**d**) Fe/γ-GY after adsorption; (**e**) Co/γ-GY after adsorption; (**f**) Ni/γ-GY after adsorption. (If the system has magnetic moment, the blue and red lines denote the spin-up and spin-down bands, respectively.)

3.4. Sensing Properties of Single 3d VIII TM Atom-Decorated γ-GY to Detect C_4F_7N

In this section, the sensing properties are evaluated based on the adsorption behavior. If TM/γ-GY is utilized as a resistance-type gas sensor, the resistance change reflects the response and sensitivity. A smaller band gap corresponds to better conductivity of the sensing material. This is because a smaller band gap indicates a smaller energy difference between the valence and conduction bands, making it easier for electrons to be excited into the conduction band and facilitate the flow of electric current. The relative conductivity σ of TM/γ-GY can be estimated as [41,42]:

$$\sigma \propto e^{[-E_g/(2k_BT)]} \tag{4}$$

where E_g, k_B, and T are the bandgap, Boltzmann's constant (8.62×10^{-5} eV/K), and Kelvin scale, respectively. Before adsorption, Fe/γ-GY and Co/γ-GY exhibit zero band gaps. However, the disappearance of the magnetic moment of Fe/γ-GY leads to the appearance of a band gap (0.31 eV), resulting in a significant decrease in the conductivity of Fe/γ-GY after C_4F_7N adsorption. On the other hand, Co/γ-GY still shows no band gap, indicating a much smaller response to C_4F_7N compared to Fe/γ-GY. In the case of Ni/γ-GY, the change

in the band gap can be neglected (0.31 eV and 0.30 eV). Therefore, the pronounced change in the band gap of Fe/γ-GY demonstrates its high sensitivity to C_4F_7N as a resistance-type gas sensor.

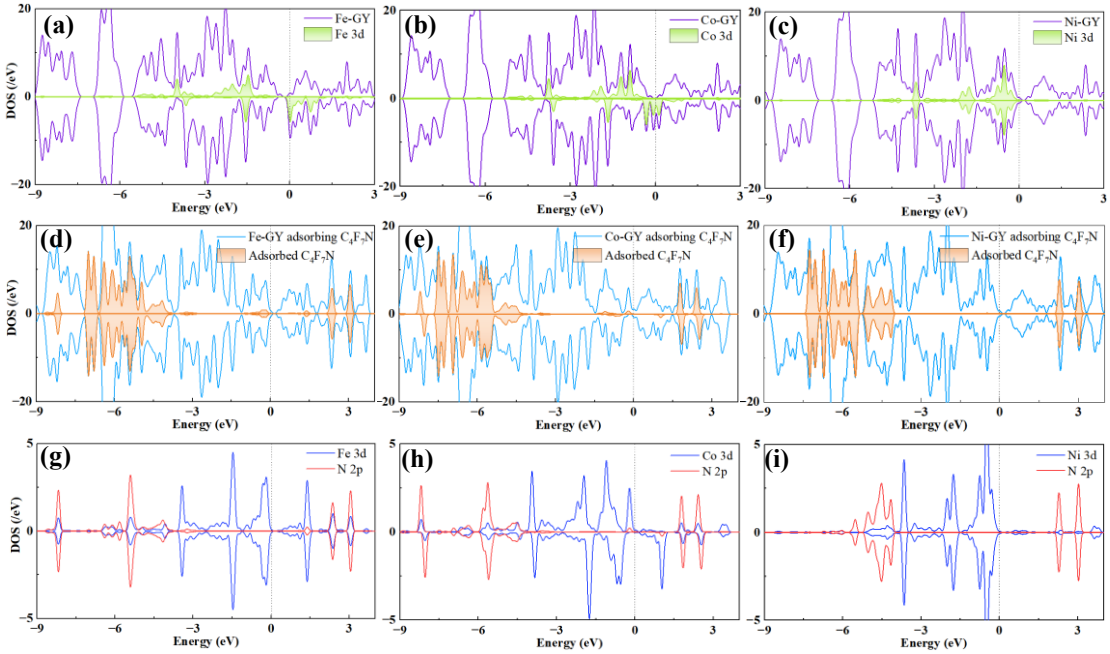

Figure 5. DOS of 3d VIII atom-decorated γ-GY before and after adsorbing C_4F_7N: (**a**) Fe/γ-GY before adsorption; (**b**) Co/γ-GY before adsorption; (**c**) Ni/γ-GY before adsorption (the purple lines are the TDOS of TM/γ-GY before adsorption, and the green shade is the TM 3d orbitals); (**d**) Fe/γ-GY after adsorption; (**e**) Co/γ-GY after adsorption; (**f**) Ni/γ-GY after adsorption (the blue lines are the TDOS of TM/γ-GY after adsorption, and the orange shade is the PDOS of adsorbed C_4F_7N); (**g**) Fe 3d and N 2p orbitals; (**h**) Co 3d and N 2p orbitals; (**i**) Ni 3d and N 2p orbitals.

Another effective method for a gas sensor is to measure the change in the work function of the sensing substrate. The value of the work function is the difference between the value of the Fermi energy and that of the electrostatic potential in a vacuum away from the surface. The work function can be calculated as [43]:

$$\Phi = U(\infty) - E_F \tag{5}$$

where Φ is the work function, $U(\infty)$ and E_F are the electrostatic potentials at the vacuum level and the Fermi energy of the sensing material. The traditional method to measure the work function is through Kelvin probe measurements. However, due to the inconvenience of the equipment and the complexity of operations, an alternative and feasible method to determine the work function change is by using metal–insulator–semiconductor (MIS) capacitors. The work function value is highly related to the drain current of the field effect transistors (FET) of MIS [44,45]. The work function values of different TM/γ-GY before and after C_4F_7N adsorption are shown in Figure 6. Prior to adsorption, the work functions of Fe/γ-GY, Co/γ-GY, and Ni/γ-GY are 5.17 eV, 5.06 eV, and 5.18 eV, respectively. After C_4F_7N adsorption, Co/γ-GY experiences the maximum increase in work function to 5.26 eV, indicating the highest response with the same adsorbing capacity. Fe/γ-GY and Ni/γ-GY exhibit smaller changes in work function, with values of 0.06 eV and 0.08 eV, respectively, indicating a lower response. Hence, if TM/γ-GY is utilized as an MIS-based work function-type gas sensor, Co/γ-GY is the most suitable sensing material for detecting C_4F_7N.

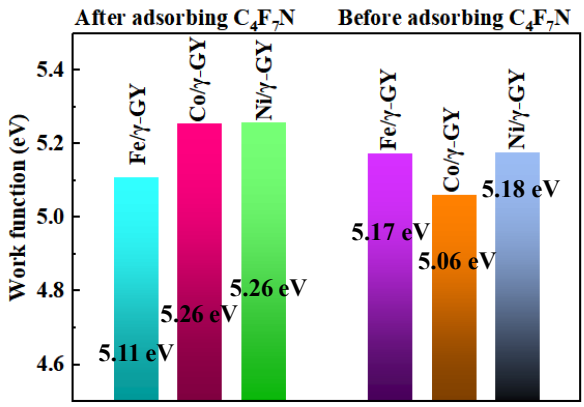

Figure 6. Work function comparison (the left three columns are the work function of TM/γ-GY after C_4F_7N adsorption while the right three columns are the work function of bare TM/γ-GY).

As a gas sensor, the recovery property is also crucial for the sensing performance. The recovery property is determined by the desorption process [46]. The desorption process can be seen as the reversed process of adsorption. The adsorption is an exothermic process, so the desorption is endothermic. Thus, desorption should overcome the energy barrier. The calculation of desorption time is inversely proportional to the desorption rate. If the adsorption energy is small, it becomes difficult for the molecule to interact with the sensing material, resulting in a weak response. On the other hand, the overlarge adsorption energy can lead to the intoxicating phenomenon of the sensing material, making desorption and repeated detection challenging. To obtain the acceptable recovery property, both the adsorption energy and the desorption energy barrier should be within a reasonable range. The desorption time can be evaluated using Van 't Hoff Arrhenius expression, which is based on the transition state theory [47,48]:

$$\tau = A^{-1} e^{(-E_{ads}/k_B T)} \tag{6}$$

where A and E_{ads} are the apparent frequency and adsorption energy. The value of A is approximated to be 10^{12} s^{-1} [47,48]. The desorption time evaluation of C_4F_7N on TM/γ-GY at different temperature are shown in Figure 7.

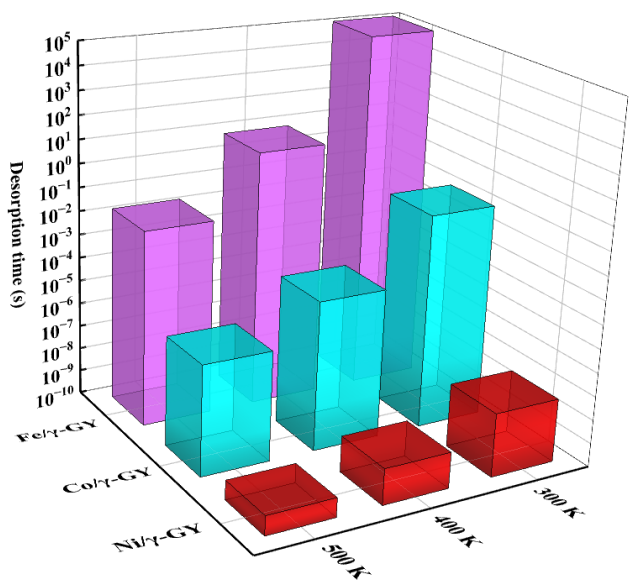

Figure 7. Desorption time of C_4F_7N on 3d VIII atom decorated γ-GY at different temperatures.

At 300 K, the desorption time of C_4F_7N on Fe/γ-GY is approximately 1.3×10^5 s, much longer than that of Co/γ-GY, which is only about 0.1 s. The difference in desorption times indicates that Co/γ-GY exhibits satisfactory recovery properties at 300 K. Furthermore, considering the work function change in Co/γ-GY, it holds great promise for the detection of C_4F_7N as a work function-type gas sensor at normal ambient temperature. As the temperature increases, the desorption time of Fe/γ-GY decreases to about 7 s at 400 K and 2×10^{-2} s at 500 K, indicating that Fe/γ-GY is more suitable for operation at higher temperatures. Considering the change in the band structure of Fe/γ-GY before and after adsorption, Fe/γ-GY performs well as a resistance-type gas sensor at higher temperatures. However, in the case of Ni/γ-GY, the desorption time is on the order of 10^{-8}, and given the weak interactions between C_4F_7N and Ni/γ-GY, the detection of C_4F_7N using Ni/γ-GY is technically unfeasible.

3.5. Thermodynamic Analysis of Adsorption Behavior

Regarding the effect of temperature on the adsorption, the adsorption free energy was calculated. The Gibbs free energy of an isolated gas molecule and adsorption system can be obtained as [49]:

$$G_{gas} = E_{ele} + E_{ZPE} + nRT - TS \tag{7}$$

$$G_{sub} = E_{ele} + E_{ZPE} + E_{C_v} - TS \tag{8}$$

where G_{gas} and G_{sub} are the Gibbs free energy of the isolated gas molecule, and TM/γ-GY before or after gas adsorption. E_{ele}, E_{ZPE}, and E_{Cv} are the electronic energy, zero-point energy (ZPE), and capacity correction. R and S signify the ideal gas constant (8.31 J/(mol·K)) and entropy of the system. The adsorption free energy is obtained as follows:

$$\Delta G_{ad} = G_{C_4F_7N\ on\ TM/\gamma\text{-}GY} - G_{TM/\gamma\text{-}GY} - G_{C_4F_7N} \tag{9}$$

Where $G_{C4F7N\ on\ TM/\gamma\text{-}GY}$, $G_{TM/\gamma\text{-}GY}$, and G_{C4F7N} are the Gibbs free energy of TM/γ-GY after adsorption, before adsorption, and isolated C_4F_7N. Thus, if ΔG_{ad} is more negative, the adsorption system is more stable. It should be noted that only the partial Hessian matrix of adsorbed C_4F_7N is calculated to obtain the vibration frequency in order to improve computing efficiency.

The relationship between temperature (300 K to 600 K) and adsorption free energy is shown in Figure 8. As the temperature increases, the adsorption free energy also increases. If the value of ΔG_{ad} is smaller than 0, the adsorption of C_4F_7N can be considered a spontaneous process. As shown in Figure 8, the intersection point of Fe/γ-GY at 0 eV is approximately 430 K, while for Co/γ-GY, it is around 330 K. On the other hand, the adsorption of Ni/γ-GY cannot occur spontaneously at room temperature. Therefore, the working temperature of TM/γ-GY should not exceed the temperature at which the adsorption process becomes spontaneous. These analyses indicate the need to evaluate the working temperature of TM/γ-GY-based gas sensors.

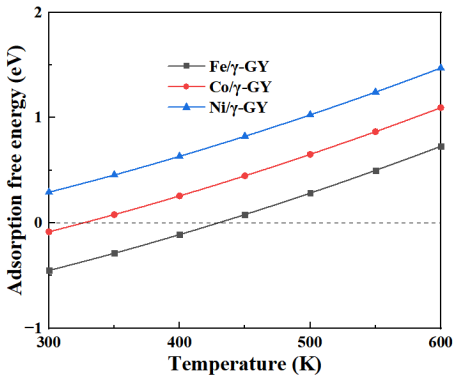

Figure 8. The adsorption free energy as a function of temperature of different TM/γ-GY systems.

4. Conclusions

In this research, the interactions between C_4F_7N and 3d VIII TM/γ-GY, as well as the sensing properties, were explored using periodic DFT calculations. Different elements of the 3d VIII TM atom were considered (Fe, Co, and Ni), and several parameters were analyzed and compared, including adsorption energy, electron transfer, and adsorption distance. The electron distribution, band structure, DOS, and work function were investigated. It was found that there is little chemical interaction between C_4F_7N and Ni atoms. However, the introduction of Fe and Co atoms enhances the chemisorption of C_4F_7N, with the Fe atom showing a greater degree of interaction. After adsorption, the magnetic moment of Fe/γ-GY vanishes, and a band gap appears. The degree of charge density difference in Fe/γ-GY is the highest, resulting in maximum electron redistribution. The chemical interactions are observed in the overlapping of TM 3d and N 2p orbitals in the DOS. Co/γ-GY exhibits the greatest change in work function after adsorbing C_4F_7N.

This research demonstrates that Fe/γ-GY has the potential to be a resistance-type gas sensor for detecting C_4F_7N, while Co/γ-GY shows promise as a work function-type sensor. Co/γ-GY is suitable for operation at room temperature, while Fe/γ-GY is more suitable for higher temperatures. Our study offers a theoretical reference for the development of C_4F_7N sensing materials and provides guidance for exploring different types of gas sensors to detect C_4F_7N and other novel insulating gases.

Author Contributions: Investigation and writing—original draft, Z.Z.; investigation, visualization, and writing—original draft, R.Z.; conceptualization, methodology, and funding acquisition, D.C.; formal analysis and data curation, Q.M.; investigation, data curation, and formal analysis, K.L.; software and resources, B.X. All authors have read and agreed to the published version of the manuscript.

Funding: This research was funded by the Natural Science Foundation of Hubei Province, grant number 2022CFB941, the Research and Innovation Initiatives of WHPU, grant number 2022Y25, the Research Funding of WHPU, grant number 2022RZ009, and the 2022 Special Subsidy Funding of WHPU, grant number 03220153.

Institutional Review Board Statement: Not applicable.

Informed Consent Statement: Not applicable.

Data Availability Statement: Not applicable.

Conflicts of Interest: The authors declare no conflict of interest.

References

1. Beroual, A.; Haddad, A. Recent advances in the quest for a new insulation gas with a low impact on the environment to replace sulfur hexafluoride (SF_6) gas in high-voltage power network applications. *Energies* **2017**, *10*, 1216. [CrossRef]
2. Osipov, A.A.; Iankevich, G.A.; Speshilova, A.B.; Osipov, A.A.; Endiiarova, E.V.; Berezenko, V.I.; Tyurikova, I.A.; Tyurikov, K.S.; Alexandrov, S.E. High-temperature etching of sic in SF_6/O_2 inductively coupled plasma. *Sci. Rep.* **2020**, *10*, 19977. [CrossRef] [PubMed]
3. Sulbaek Andersen, M.P.; Kyte, M.; Andersen, S.T.; Nielsen, C.J.; Nielsen, O.J. Atmospheric chemistry of (cf3)2cf–c≡n: A replacement compound for the most potent industrial greenhouse gas, SF_6. *Environ. Sci. Technol.* **2017**, *51*, 1321–1329. [CrossRef]
4. Li, X.; Zhao, H.; Murphy, A.B. SF_6-alternative gases for application in gas-insulated switchgear. *J. Phys. D Appl. Phys.* **2018**, *51*, 153001. [CrossRef]
5. Li, Y.; Zhang, X.; Xiao, S.; Chen, Q.; Tang, J.; Chen, D.; Wang, D. Decomposition properties of C_4F_7N/N_2 gas mixture: An environmentally friendly gas to replace SF_6. *Ind. Eng. Chem. Res.* **2018**, *57*, 5173–5182. [CrossRef]
6. Kieffel, Y.; Irwin, T.; Ponchon, P.; Owens, J. Green gas to replace SF_6 in electrical grids. *IEEE Power Energy Mag.* **2016**, *14*, 32–39. [CrossRef]
7. Xiao, S.; Chen, D.; Tang, J.; Li, Y. Adsorption behavior of γ-Al_2O_3 toward heptafluoroisobutyronitrile and its decompositions: Theoretical and experimental insights. *IEEE Access* **2020**, *8*, 36741–36748. [CrossRef]
8. Chen, L.; Zhang, B.; Yang, T.; Deng, Y.; Li, X.; Murphy, A.B. Thermal decomposition characteristics and kinetic analysis of C_4F_7N/CO_2 gas mixture. *J. Phys. D Appl. Phys.* **2020**, *53*, 055502. [CrossRef]
9. *Material Toxicity Summary Sheet, 3M™ Novec™ 4710 Insulating Gas*; 3M Company: St. Paul, MN, USA, 2019.
10. Li, Y.; Zhang, X.; Zhang, J.; Xiao, S.; Xie, B.; Chen, D.; Gao, Y.; Tang, J. Assessment on the toxicity and application risk of C_4F_7N: A new SF_6 alternative gas. *J. Hazard. Mater.* **2019**, *368*, 653–660. [CrossRef]

11. Guo, Y.; Xu, K.; Wu, C.; Zhao, J.; Xie, Y. Surface chemical-modification for engineering the intrinsic physical properties of inorganic two-dimensional nanomaterials. *Chem. Soc. Rev.* **2015**, *44*, 637–646. [CrossRef]
12. Sun, P.; Wang, K.; Zhu, H. Recent developments in graphene-based membranes: Structure, mass-transport mechanism and potential applications. *Adv. Mater.* **2016**, *28*, 2287–2310. [CrossRef] [PubMed]
13. Tian, W.; Liu, X.; Yu, W. Research progress of gas sensor based on graphene and its derivatives: A review. *Appl. Sci.* **2018**, *8*, 1118. [CrossRef]
14. Chen, Z.; Wang, J.; Wang, Y. Strategies for the performance enhancement of graphene-based gas sensors: A review. *Talanta* **2021**, *235*, 122745. [CrossRef]
15. Kharche, N.; Nayak, S.K. Quasiparticle band gap engineering of graphene and graphone on hexagonal boron nitride substrate. *Nano Lett.* **2011**, *11*, 5274–5278. [CrossRef] [PubMed]
16. Li, H.; Lim, J.H.; Lv, Y.; Li, N.; Kang, B.; Lee, J.Y. Graphynes and graphdiynes for energy storage and catalytic utilization: Theoretical insights into recent advances. *Chem. Rev.* **2023**, *123*, 4795–4854. [CrossRef] [PubMed]
17. Narita, N.; Nagai, S.; Suzuki, S.; Nakao, K. Optimized geometries and electronic structures of graphyne and its family. *Phys. Rev. B* **1998**, *58*, 11009–11014. [CrossRef]
18. Li, Q.; Li, Y.; Chen, Y.; Wu, L.; Yang, C.; Cui, X. Synthesis of γ-graphyne by mechanochemistry and its electronic structure. *Carbon* **2018**, *136*, 248–254. [CrossRef]
19. Hu, Y.; Wu, C.; Pan, Q.; Jin, Y.; Lyu, R.; Martinez, V.; Huang, S.; Wu, J.; Wayment, L.J.; Clark, N.A.; et al. Synthesis of γ-graphyne using dynamic covalent chemistry. *Nat. Synth.* **2022**, *1*, 449–454. [CrossRef]
20. Kim, S.; Ruiz Puigdollers, A.; Gamallo, P.; Viñes, F.; Lee, J.Y. Functionalization of γ-graphyne by transition metal adatoms. *Carbon* **2017**, *120*, 63–70. [CrossRef]
21. He, J.; Zhou, P.; Jiao, N.; Ma, S.Y.; Zhang, K.W.; Wang, R.Z.; Sun, L.Z. Magnetic exchange coupling and anisotropy of 3d transition metal nanowires on graphyne. *Sci. Rep.* **2014**, *4*, 4014. [CrossRef]
22. Chen, D.; Zhang, X.; Tang, J.; Cui, H.; Li, Y.; Zhang, G.; Yang, J. Density functional theory study of small Ag cluster adsorbed on graphyne. *Appl. Surf. Sci.* **2019**, *465*, 93–102. [CrossRef]
23. Lu, Z.; Lv, P.; Ma, D.; Yang, X.; Li, S.; Yang, Z. Detection of gas molecules on single mn adatom adsorbed graphyne: A dft-d study. *J. Phys. D Appl. Phys.* **2018**, *51*, 065109. [CrossRef]
24. Ma, D.W.; Li, T.; Wang, Q.; Yang, G.; He, C.; Ma, B.; Lu, Z. Graphyne as a promising substrate for the noble-metal single-atom catalysts. *Carbon* **2015**, *95*, 756–765. [CrossRef]
25. He, C.; Wang, R.; Xiang, D.; Li, X.; Fu, L.; Jian, Z.; Huo, J.; Li, S. Charge-regulated CO_2 capture capacity of metal atom embedded graphyne: A first-principles study. *Appl. Surf. Sci.* **2020**, *509*, 145392. [CrossRef]
26. Li, S.-L.; Li, Q.; Chen, Y.; Zhao, Y.; Gan, L.-Y. Transition metal embedded graphynes as advanced bifunctional single atom catalysts for oxygen reduction and evolution reactions. *Appl. Surf. Sci.* **2022**, *605*, 154828. [CrossRef]
27. Gao, X.; Zhou, Y.; Tan, Y.; Liu, S.; Cheng, Z.; Shen, Z. Graphyne doped with transition-metal single atoms as effective bifunctional electrocatalysts for water splitting. *Appl. Surf. Sci.* **2019**, *492*, 8–15. [CrossRef]
28. Delley, B. From molecules to solids with the $DMol^3$ approach. *J. Chem. Phys.* **2000**, *113*, 7756–7764. [CrossRef]
29. Perdew, J.P.; Chevary, J.A.; Vosko, S.H.; Jackson, K.A.; Pederson, M.R.; Singh, D.J.; Fiolhais, C. Atoms, molecules, solids, and surfaces: Applications of the generalized gradient approximation for exchange and correlation. *Phys. Rev. B* **1992**, *46*, 6671–6687. [CrossRef]
30. Perdew, J.P.; Burke, K.; Ernzerhof, M. Generalized gradient approximation made simple. *Phys. Rev. Lett.* **1996**, *77*, 3865–3868. [CrossRef]
31. Grimme, S. Semiempirical GGA-type density functional constructed with a long-range dispersion correction. *J. Comput. Chem.* **2006**, *27*, 1787–1799. [CrossRef]
32. Monkhorst, H.J.; Pack, J.D. Special points for Brillouin-zone integrations. *Phys. Rev. B* **1976**, *13*, 5188. [CrossRef]
33. Hirshfeld, F.L. Bonded-atom fragments for describing molecular charge densities. *Theor. Chem. Acta* **1977**, *44*, 129–138. [CrossRef]
34. Zhang, X.; Li, Y.; Chen, D.; Xiao, S.; Tian, S.; Tang, J.; Wang, D. Dissociative adsorption of environment-friendly insulating medium C_3F_7CN on Cu(111) and Al(111) surface: A theoretical evaluation. *Appl. Surf. Sci.* **2018**, *434*, 549–560. [CrossRef]
35. Fu, Y.; Yang, A.; Wang, X.; Rong, M. Theoretical study of the decomposition mechanism of C_4F_7N. *J. Phys. D Appl. Phys.* **2019**, *52*, 245203. [CrossRef]
36. Ruiz-Puigdollers, A.; Gamallo, P. Dft study of the role of n- and b-doping on structural, elastic and electronic properties of α-, β- and γ-graphyne. *Carbon* **2017**, *114*, 301–310. [CrossRef]
37. Guo, Y.; Chen, Z.; Wu, W.; Liu, Y.; Zhou, Z. Adsorption of nox (x = 1, 2) gas molecule on pristine and b atom embedded γ-graphyne based on first-principles study. *Appl. Surf. Sci.* **2018**, *455*, 484–491. [CrossRef]
38. Philipsen, P.H.T.; Baerends, E.J. Cohesive energy of 3d transition metals: Density functional theory atomic and bulk calculations. *Phys. Rev. B* **1996**, *54*, 5326–5333. [CrossRef] [PubMed]
39. Bendavid, L.I.; Carter, E.A. CO_2 adsorption on Cu_2O(111): A DFT+U and DFT-D study. *J. Phys. Chem. C* **2013**, *117*, 26048–26059. [CrossRef]
40. Kou, L.; Frauenheim, T.; Chen, C. Phosphorene as a superior gas sensor: Selective adsorption and distinct I–V response. *J. Phys. Chem. Lett.* **2014**, *5*, 2675–2681. [CrossRef]

41. Wu, Y.; Chen, X.; Weng, K.; Arramel; Jiang, J.; Ong, W.-J.; Zhang, P.; Zhao, X.; Li, N. Highly sensitive and selective gas sensor using heteroatom doping graphdiyne: A DFT study. *Adv. Electron. Mater.* **2021**, *7*, 2001244. [CrossRef]
42. Chen, D.; Zhang, X.; Tang, J.; Cui, Z.; Cui, H. Pristine and cu decorated hexagonal inn monolayer, a promising candidate to detect and scavenge sf6 decompositions based on first-principle study. *J. Hazard. Mater.* **2019**, *363*, 346–357. [CrossRef] [PubMed]
43. Lu, Z.; Zhai, Y.; Liang, Q.; Wu, W. Promoting sensitivity and selectivity of NO_2 gas sensor based on metal (Pt, Re, Ta)-doped monolayer WSe_2: A DFT study. *Chem. Phys. Lett.* **2020**, *755*, 137737. [CrossRef]
44. Flietner, B.; Doll, T.; Lechner, J.; Leu, M.; Eisele, I. Reliable hybrid GasFETs for work-function measurements with arbitrary materials. *Sens. Actuators B* **1994**, *22*, 109–113. [CrossRef]
45. Eisele, I.; Doll, T.; Burgmair, M. Low power gas detection with FET sensors. *Sens. Actuators B* **2001**, *78*, 19–25. [CrossRef]
46. Luo, H.; Zhang, L.; Xu, S.; Shi, M.; Wu, W.; Zhang, K. NH_3, PH_3 and AsH_3 adsorption on alkaline earth metal (Be-Sr) doped graphenes: Insights from DFT calculations. *Appl. Surf. Sci.* **2021**, *537*, 147542. [CrossRef]
47. Peng, S.; Cho, K.; Qi, P.; Dai, H. Ab initio study of CNT NO_2 gas sensor. *Chem. Phys. Lett.* **2004**, *387*, 271–276. [CrossRef]
48. Zhang, Y.-H.; Chen, Y.-B.; Zhou, K.-G.; Liu, C.-H.; Zeng, J.; Zhang, H.-L.; Peng, Y. Improving gas sensing properties of graphene by introducing dopants and defects: A first-principles study. *Nanotechnology* **2009**, *20*, 185504. [CrossRef]
49. Gao, Z.; Li, L.; Huang, H.; Xu, S.; Yan, G.; Zhao, M.; Ding, Z. Adsorption characteristics of acid gases (NO, NO_2, SO_2 and SO_3) on different single-atom nickel adsorbent: A first-principles study. *Appl. Surf. Sci.* **2020**, *527*, 146939. [CrossRef]